Chapter 3

The experimental system: description, experimental characterization, and sample preparation

This chapter will introduce the investigated system consisting of derivatives of perylene and nano-structured TiO_2 anatase. The system is characterized by experimental as well as theoretical methods. Finally the preparation of the samples will be described. It has been found that details of the preparation procedure affect the microscopic properties of the system.

3.1 The chromophores: derivatives of perylene

3.1.1 Properties of the neutral chromophores

The chromophores investigated throughout this study are derivatives of the polycyclic aromatic hydrocarbon perylene $C_{20}H_{12}$. Perylene has been chosen as a model dye for the investigation of heterogeneous ET mainly for two reasons.
First, the absorption spectra of the electronic states involved in the ET process, i.e. the ground state and the excited state absorption of the neutral chromophore as well as the ground state absorption of the oxidized dye (product of the ET reaction), are well separated. Additionally, the transitions are in the visible spectral range (Fig. 3.1). These absorption characteristics, which have been discussed extensively in Refs. [12, 117, 118, 106, 17], allow the direct spectroscopic investigation of the ET process with a two-color pump-probe experiment. Secondly, there are no ultrafast decay channels of the first excited singlet state for the free molecule. The fluorescence quantum yield is above 90% [119, 120]. Therefore electron injection

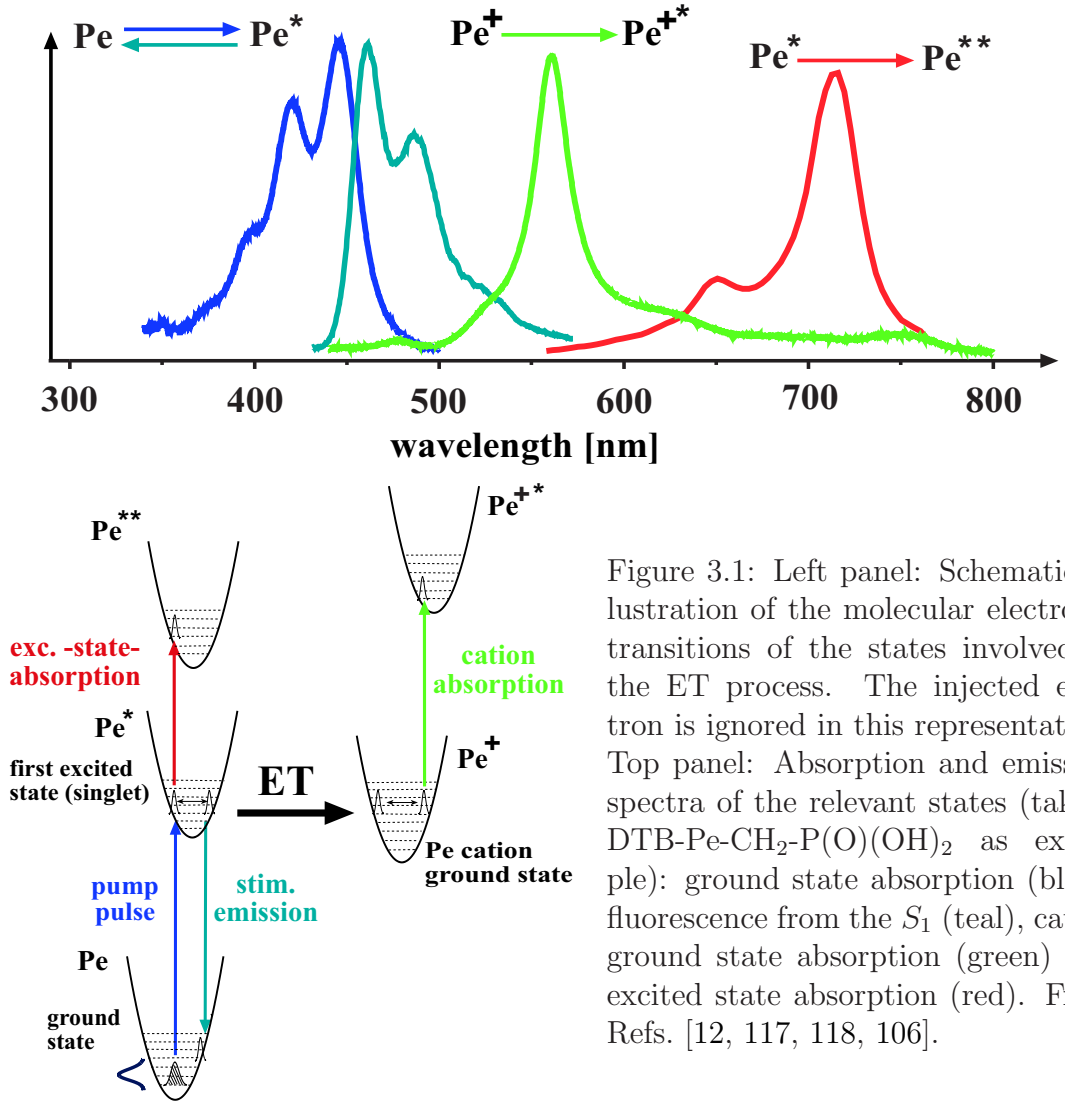

Figure 3.1: Left panel: Schematic illustration of the molecular electronic transitions of the states involved in the ET process. The injected electron is ignored in this representation. Top panel: Absorption and emission spectra of the relevant states (taking DTB-Pe-CH_2-P(O)$(OH)_2$ as example): ground state absorption (blue), fluorescence from the S_1 (teal), cation ground state absorption (green) and excited state absorption (red). From Refs. [12, 117, 118, 106].

is the only ultrafast electronic reaction for the chromophore on the surface. The combination of these two features is rather unique, making perylene an ideal model dye for this investigation.

3.1.1.1 Electronic properties of neutral perylene

First, some fundamental properties of perylene will be discussed. The ground state absorption above 350 nm arises from the Franck-Condon progression of the $S_0(^1A_g) \rightarrow S_1(^1B_{1u})$ transition (transition symmetry B_{3u}, molecular point group D_{2h}) [121, 122]. There is no excitation to higher excited states or from lower lying states in that spectral range. Halasinski *et al.* investigated the electronic absorption spectra of perylene and its positive and negative ion spectroscopically and theoretically [122, 123]. Fig. 3.2, taken from that reference, shows the HOMO and the

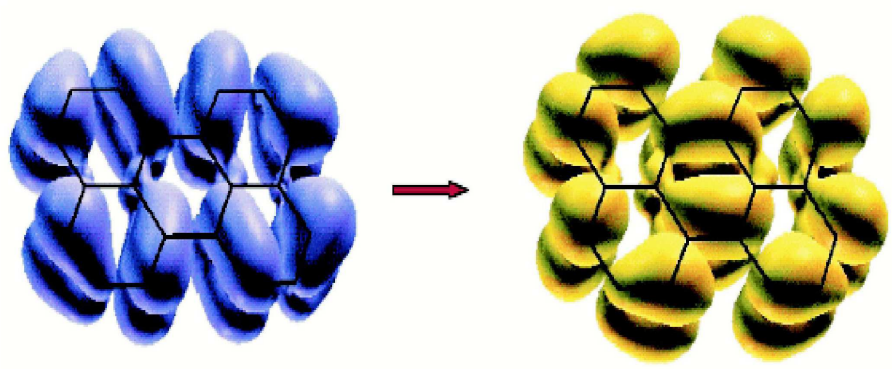

Figure 3.2: HOMO (left) and excited state (right) of the neutral perylene obtained with a TDDFT calculation. These states visualize the $S_0(^1A_g) \rightarrow S_1(^1B_{1u})$ transition (taken from Ref. [122]).

excited state of the neutral perylene obtained from time-dependent density functional theory (TDDFT) calculations. According to this analysis, the $S_0(^1A_g) \rightarrow S_1(^1B_{1u})$ transition of neutral perylene is an almost pure (to 98.4%) HOMO to LUMO transition. This arises from a large energetic separation of the HOMO from the HOMO-1 and of the LUMO from the LUMO+1, each about 1.5 eV. Within the scope of this thesis semi-empirical MO calculations have been applied (see appendix A.1 for details). The low computational costs of these calculations allow the modeling of large chromophores on a personal computer. The reliability of these methods was checked on the basis of different criteria. For instance, the same electronic transition as shown in Fig. 3.2 was found to be in good agreement with the TDDFT calculations[1].

As the $S_0(^1A_g) \rightarrow S_1(^1B_{1u})$ transition has strong HOMO→LUMO character, the excited state wavefunction is in a very good approximation represented by the LUMO wavefunction. However, this is not the case for the eigenvalue. The energy of the LUMO mainly reflects the energy of an additional electron in the molecule. The difference between the vacuum level and the LUMO eigenvalue gives an approximation of the electron affinity (EA) of the molecule rather than the excited state energy [125]. The latter can be estimated best from the position of the HOMO plus the excitation energy of the transition obtained from a CI calculation [126].
In chapter 4, the observed kinetics of the ET from the excited state will be qualitatively discussed in terms of the excited state wavefunction. The specified electronic

[1]Semi-empirical configuration interaction (CI) ZINDO/S calculations reveal pure (100%) HOMO-LUMO contributions to the $S_0(^1A_g) \rightarrow S_1(^1B_{1u})$ transition. The transition energy is overestimated with respect to the experimental value [122] by about 10%, whereas TDDFT calculations underestimate the transition energy by about 10%. The characters of the wavefunctions are usually well reproduced by semi-empirical methods. With respect to the molecular structure semi-empirical calculations underestimate the bond length by about 1%, whereas relative bond length and bond angles are excellently reproduced (results compared with DFT calculation of Ref. [124]).

properties of perylene legitimate the consideration of the LUMO wavefunction in combination with the CI eigenvalue as excited state.

3.1.1.2 Investigated perylene derivatives

All investigated dyes were perylene species substituted by three organic groups covalently bound to the chromophore. Two bulky tertiary-butyl groups in the 2- and 5-position prevent a strong interaction of the π-systems of neighboring molecules and therefore the formation of dimers [127]. This warrants that single molecules are investigated on the surface.

The linkage to the semiconductor surface was achieved by an acid group, which is directly or via bridge units bound to the perylene body in 9-position. It will be called the anchor group in the following. Two different acid groups were investigated, namely carboxylic and phosphonic acids, as shown in Fig. 3.3. The electronic coupling between the dye and the surface is expected to depend on factors like the spatial arrangement of the chromophore, the nature of anchor-surface bonding, and the electronic structure of the molecular unit providing the covalent bonds. To address these factors, bridge units were inserted between the perylene skeleton and the acid group. The chemical nature of the different bridge units is discussed in chapter 4 in the context of the observed ET kinetics.

The perylene derivatives were synthesized starting from naphthalene by W. Storck (Fritz-Haber-Institut Berlin, HMI Berlin) and S. Felber (HMI Berlin). Details of the synthesis can be found in Refs. [19, 128]. The tripod unit was provided by the group of E. Galoppini, Rutgers University, and linked with the chromophore by S. Felber [129].

The absorption and emission spectra of the perylene dyes in solution are summarized in Fig. 3.4. The 0-0 transition energies are estimated from the intersection of the normalized absorption and emission spectra and are given in the figure's caption. The spectra of the dye with electronically saturated bridge-anchor units are very similar. The transition energies of DTB-Pe-CH=CH-COOH and DTB-Pe-tripod are red-shifted by about 1200 cm^{-1}, as the ethylene group (acrylic acid) and accordingly the acetyl group (tripod) are involved in the transition. Metaphorically speaking, the excited state wavefunctions spread into the bridge unit. A larger delocalization usually results in a lowering of the eigenvalue, which manifests in a red-shift of the optical transitions. This bridge effect is discussed in detail in section 4.

Fig. 3.5 gives an impression of the wavefunctions of HOMO and LUMO/excited state. Exemplary DTB-Pe-COOH is considered, in comparison to the LUMO of the pure perylene. The following characteristics should be noted:

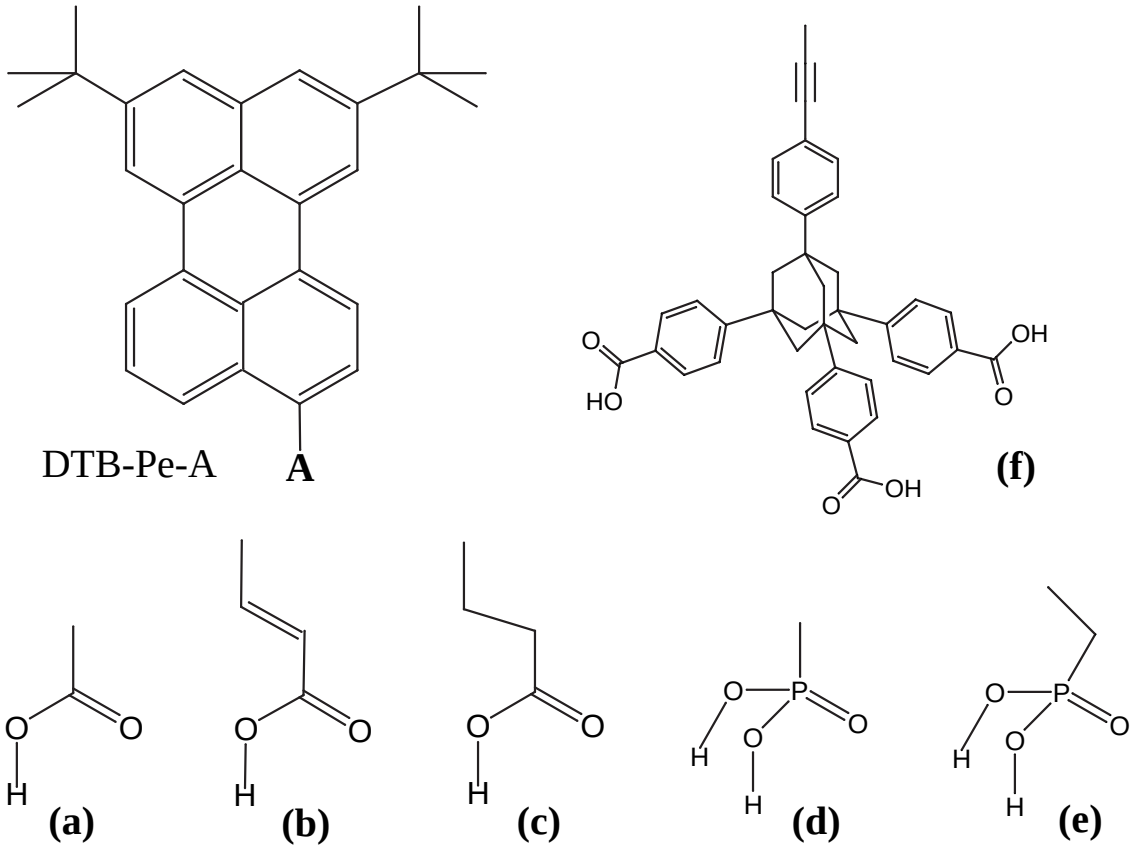

Figure 3.3: Structural formulas of the investigated chromophores. The core chromophore, 2,5-Di-tert-butyl-perylen-9-yl (DTB-Pe-A) is linked with one of the bridge-anchor groups (a-f) at position A: "carboxylic acid" -COOH (a), "acrylic acid" -CH=CH-COOH (b), "propionic acid" -CH_2-CH_2-COOH (c), "phosphonic acid" -P(O)$(OH)_2$ (d), "methyl phosphonic acid" -CH_2-P(O)$(OH)_2$ (e) and "-tripod" (f).

- The wavefunctions of both, HOMO and LUMO, have strong $\pi/\pi^\star$-character and are delocalized over the perylene skeleton, very similar to the analogous states of pure perylene. This is also reflected by the similarity of the transition dipole $\boldsymbol{\mu}$ and the oscillator strength f for both molecules: perylene: $\mu_1 = -7.3, \mu_2 = -4.2, \mu_3 = 0.0, f = 0.87$ (experimental value: $f = 0.81$) [119]; DTB-Pe-COOH: $\mu_1 = -7.4, \mu_2 = -5.2, \mu_3 = 0.9, f = 0.96$[2].

- The wavefunctions spread into the anchor group to a certain extent. For all investigated perylene derivatives, this effect is stronger for the excited state compared to the HOMOs. A measure for the spatial charge rearrangement attending the optical transition is the electric dipole $\boldsymbol{p}_{exc}$ of the excited state (CI calculation) compared to the total dipole $\boldsymbol{p}_{tot}$ of the non-excited molecule:

[2] μ_{1-3} denote the components of the $S_0(^1A_g) \rightarrow S_1(^1B_{1u})$ transition dipole along the inertial axes of the molecule. The axes refer approximately to the long molecular in-plane axis (1), the short in-plane axis (2), and normal to the perylene plane (3) (see appendix A.2 for details).

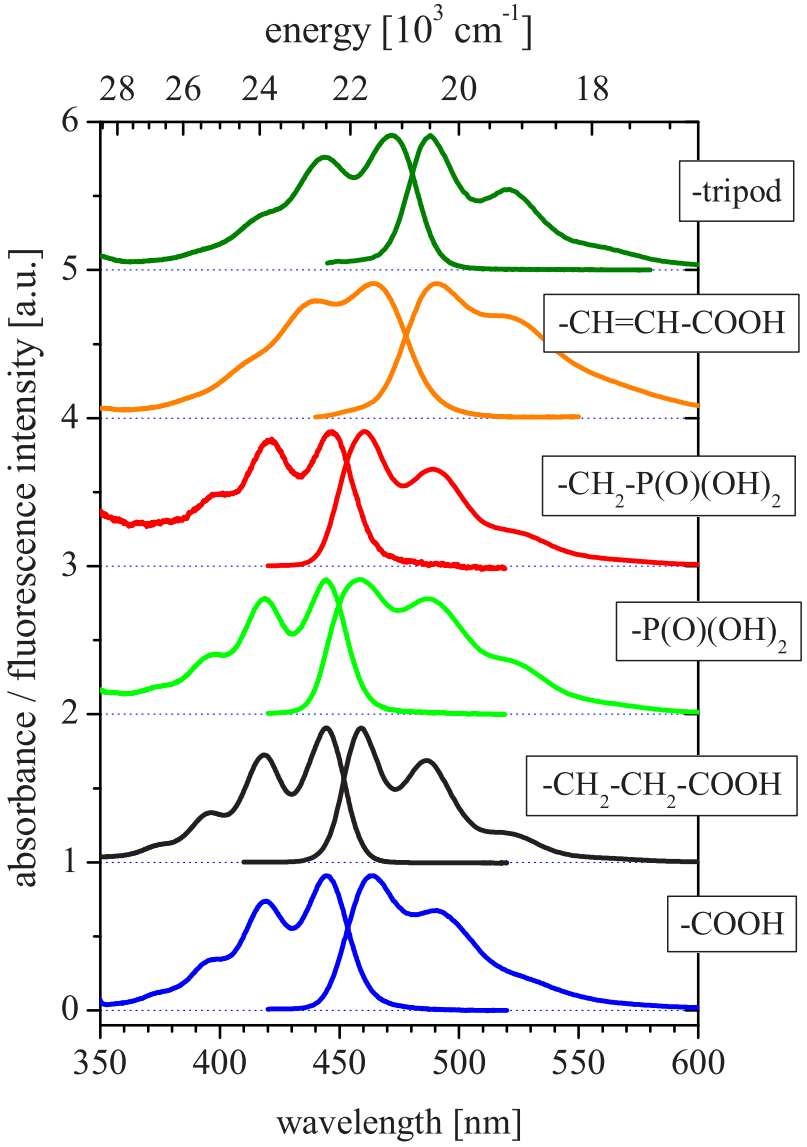

Figure 3.4: Normalized absorption and emission spectra of the perylene chromophores in solution. The molecules were dissolved in 1:1 toluene:methanol. The absorption spectra were recorded for solutions with dye concentrations around 10^{-5}M. The emission spectra are taken at dye-concentrations of about 10^{-6}M with excitation at 410 nm. The 0-0 transition energies (wavelength) are: DTB-Pe-COOH: 22080 cm^{-1} (453 nm); DTB-Pe-CH_2-CH_2-COOH: 22150 cm^{-1} (451.5 nm); DTB-Pe-P(O)$(OH)_2$: 22200 cm^{-1} (450 nm); DTB-Pe-CH_2-P(O)$(OH)_2$: 22080 cm^{-1} (453 nm); DTB-Pe-CH=CH-COOH: 20950 cm^{-1} (477.5 nm); DTB-Pe-Tripod: 20830 cm^{-1} (480 nm). The red-shift of the transitions of DTB-Pe-CH=CH-COOH and DTB-Pe-tripod arises from the molecular units next to the chromophore. In both molecules an electronically unsaturated molecular unit with sp^2-hybridization (acrylic acid) and *sp*-hybridization (tripod) is incorporated in the excited state wavefunction. Semi-empirical calculations reveal the spectral shifts quantitatively correct.

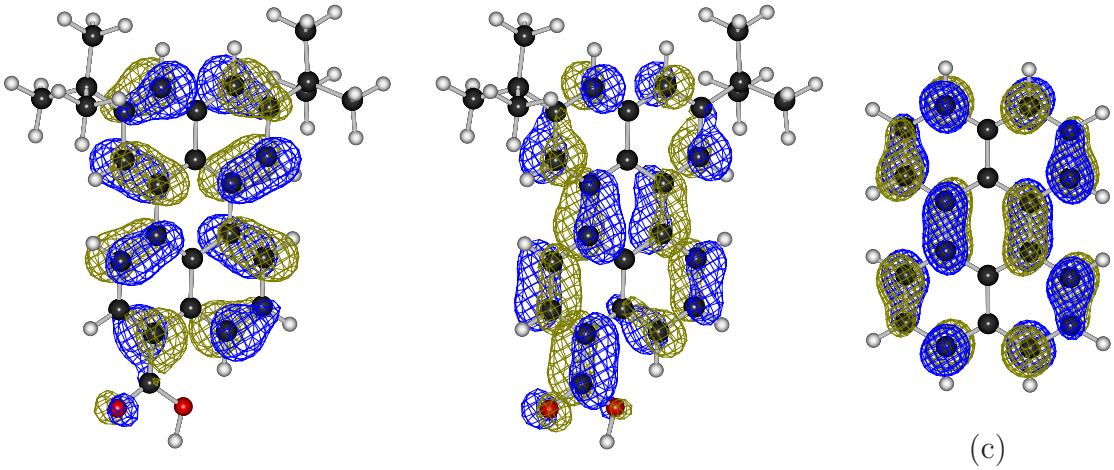

(a) (b) (c)

Figure 3.5: Neutral DTB-Pe-COOH: HOMO [E = -7.0 eV] (a), LUMO [E = -1.3 eV] (b), and neutral perylene LUMO [E = -0.8 eV] (c) (RHF ZINDO/S calculation).

$\boldsymbol{p}_{exc}$ = 10.4 D ($p_1 = -4.5, p_2 = -9.4, p_3 = -0.8$) $\boldsymbol{p}_{tot}$ = 4.8 D ($p_1 = -2.4, p_2 = -4.1, p_3 = -0.4$), i.e. $\Delta\boldsymbol{p}$ = 5.7 D ($\Delta p_1 = 2.1, \Delta p_2 = 5.3, \Delta p_3 = 0.4$). Thus, the optical transition causes a slight electronic rearrangement toward the anchor group.

- In a good approximation the tertiary butyl groups are "electronically inert" with respect to the HOMO and the LUMO. This holds also for the HOMOs and the LUMOs of the oxidized molecule (Fig. A.1). Therefore, the bulky groups fulfill the requirement of preventing dimer formation without significantly affecting the electronic levels of interest.

3.1.2 Excited state lifetime of the free molecule

As mentioned in the beginning of this chapter, the absence of ultrafast decay processes of the photo-excited state is important for an unambiguous study of the ET process. The investigation of transition metal-organic dyes, which are the most relevant sensitizers for solar energy conversion, is obstructed by a very efficient intersystem crossing (ISC) from the photo-excited singlet to the lowest-energy triplet metal-to-ligand charge transfer (^{3}MLCT) excited state. Sundström and co-workers reported a time constant of 75 fs for the ^{1}MLCT→^{3}MLCT transition, competing with the ET from the singlet state with a time constant of 50 fs [22]. An additional complication arises from the complex nature of the excited singlet state itself: as there are up to three equivalent ligands, the excited state is a superposition of several electronic states, which are almost degenerated. This superposition evolves in time,

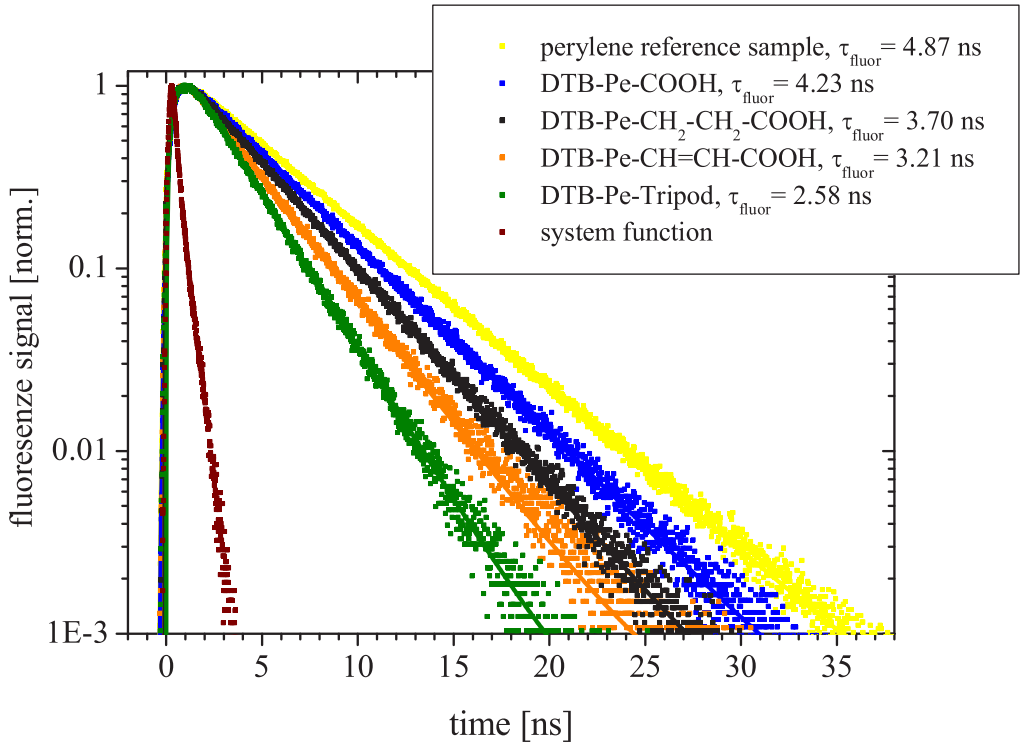

Figure 3.6: Time-resolved fluorescence at 480 nm of different perylene chromophores with carboxylic groups.

for instance in the form of a localization of the initially delocalized wavefunction on one single ligand [84]. The final complications for a spectroscopic investigation of that system are the broad and overlapping absorption spectra of the different electronic states.

The electronic structure and the excited state kinetics of perylene is much simpler. The lifetime of the excited singlet state for pure perylene is around 5 ns, and the decay is mainly radiative. Fluorescence quantum yields of 97% in the gas phase [120] and of 93% in solution [119] have been reported. ISC to the triplet can be neglected as it occurs with a time constant of 330 ns [119]. To ensure that this behavior is not altered by the substituted groups, the fluorescenece lifetime of the derivatives has been determined with time-correlated single photon counting (SPC). Details of the measurement are given in appendix A.3.1. Fig. 3.6 shows the decay of the fluorescence detected within a spectral window of 10 nm around 480 nm for the dyes containing carboxylic groups in comparison to a perylene fluorescence standard. The $S_0(^1A_g) \rightarrow S_1(^1B_{1u})$ transition was pumped with a femtosecond pulse around 400 nm. All decay curves in Fig. 3.6 show mono-exponential behavior over three decades. The time constants obtained from the fit are given in the legend.

Interestingly, the fluorescence lifetime seems to correlate with the size of the bridge-anchor unit, in particular if the shape of the excited state wavefunctions is con-

sidered. The delocalization is strongest for DTB-Pe-CH=CH-COOH and DTB-Pe-tripod due to the electronically unsaturated bridge group next to the perylene ring system. However, both perylene phosphonic acids (not plotted) deviate from this trend, as the fluorescence of DTB-Pe-P(O)$(OH)_2$ and DTB-Pe-CH_2-P(O)$(OH)_2$ decays with 3.8 ns and 5.1 ns, respectively. Independent from the microscopic origin of this variation by up to the factor of two, the important conclusion from Fig. 3.6 is that the rate of the concurring decay process is below 10^9/s for all dyes under investigation.

3.1.3 Properties of the oxidized chromophores

3.1.3.1 Electronic transitions

The products of the heterogeneous ET reaction are the oxidized chromophore and the electron in the semiconductor. The transient absorption of the oxidized dye is the preferred probe signal in the time-resolved studies of the electron injection. Therefore, the physics of this transition will be discussed.

The perylene cation absorption was measured with different methods for the generation of the oxidized state:

- Stationary oxidation by H_2SO_4 [130, 117].
- Transient oxidation in a Ne matrix at 4 K under *in situ* UV illumination [131].
- Transient oxidation by intermolecular ET in solution [132, 117].
- Transient oxidation on TiO_2 [117].

Generally speaking, the cation spectrum exhibits a narrow absorption band around 550 nm, the exact peak position and its width depend on the environment. The band has been assigned to a $D_0(^2A_u) \rightarrow D_5(^2B_{3g})$ transition [131]. Lower transitions around 750 nm have weak oscillator strength (see Fig. 3.1). Burfeindt [117] investigated the influence of the substituents for DTB-Pe-CH_2-P(O)$(OH)_2$ on the cation absorption and observed a slight red-shift of about 20 nm compared to pure perylene.

Microscopic insight into the transition is obtained by the TDDFT calculations of Halasinski *et al.* [122]. The electronic structure of the ion has to be considered in an open-shell picture (UHF calculation), that means that spin-up (α) and spin-down (β) electrons are considered separately. Similar to the excitation of neutral perylene, the strong transition around 550 nm has mainly (98.1%) HOMO-LUMO character, but with contributions from both electron subspaces ($HOMO_\alpha \rightarrow LUMO_\alpha$: 44.3%,

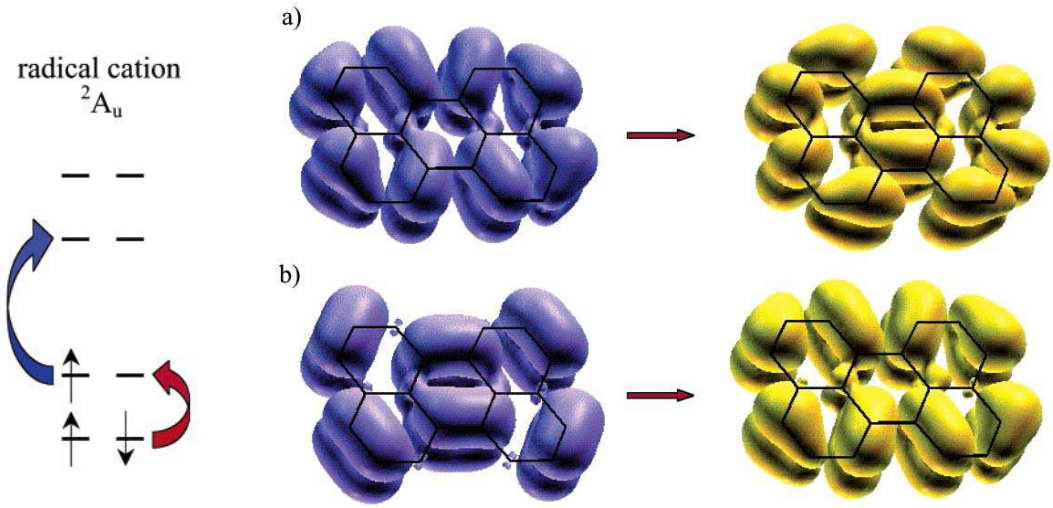

Figure 3.7: Left: schematic diagram of the HOMO-LUMO transitions in both α and β electron spaces. Right: perylene radical cation TDDFT calculations. (a) α and (b) β electron attachment/detachment densities (representing the charge density moving during the excitation) of the $^2A_u \rightarrow ^2B_{3g}$ transition. From Ref. [122].

$\text{HOMO}_\beta \rightarrow \text{LUMO}_\beta$: 53.8%). Fig. 3.7 visualizes the optical transition by means of electron attachment/detachment densities, which represent the charge density moving during the transition. The α transition shows strong similarities with the HOMO-LUMO transition of the neutral molecule. It should be noted that semi-empirical UHF ZINDO/S calculations of the perylene cation reproduce the four wavefunctions mostly involved in the cation excitation remarkably well. This establishes confidence in the semi-empirical calculations of the oxidized perylene derivatives studied in this thesis.

In chapter 4, the rise of the cation absorption is used as probe of the ET reaction. As outlined in chapter 1, heterogeneous ET in the adiabatic limit can become a purely electronic process elapsing at almost "frozen" nuclear configuration. It is questionable if both subsequent electronic processes, i.e. optical excitation and ET, can be considered as instantaneous processes without inherent dynamics. If the ET reaction is regarded as electron "motion" from the molecule into the surface, the question poses, at which point of this electron "motion" the molecule can be considered as cation. In view of this aspect, the visualization of the perylene cation absorption in Fig. 3.7 should be helpful. All four involved states are delocalized over the whole perylene backbone. Thus, the appearance of the characteristic cation absorption band around 570 nm indicates that the photoexcited electron left the perylene backbone and the electronic structure has changed to that of the perylene cation ground state. Therefore, in the case of perylene the cation absorption can be regarded as a proper measure of the ET product. This conclusion can not be generalized. For example transitions between intramolecular localized wavefunctions

might be rather insensitive to electron dynamics occurring in a different molecular subunit.

3.1.3.2 Vibrational relaxation

A photo-induced electronic transition usually excites the molecule also vibrationally. The temporal evolution of the vibrational population is a research field apart and has been studied for several systems (see for example [40] and references therein). The kinetics of the vibrational cooling strongly depends both on molecular and solvent properties, wherefore the observed vibrational population relaxation times T_1 range from sub-1 ps to hundreds of picoseconds. Jiang and Blanchard have studied perylene in n-alkanes and measured the decay of the ν_7 mode (1375 cm^{-1}), which is Raman active and the strongest contribution to the second peak in the absorption spectrum of perylene (Fig. 3.1, [124]). This mode fades out with a 140 ps time constant in nonpolar solvents. The ET times observed in this thesis are up to 10^4 faster than the vibrational relaxation.

If the initially generated vibrational population is a coherent superposition (vibrational wavepacket), the decay of the coherence is of interest as well. Zimmermann *et al.* have studied the vibrational dephasing for perylene in solution and linked to TiO_2, and addressed the influence of a wavepacket on the heterogeneous ET [106, 19]. For the free dye in solution, the wavepacket was found up to 1.5 ps. Thus, the ET does not only occur from a vibrationally hot, but even from a vibrationally coherent molecule. As discussed in the introduction, Ramakrishna, Willig, and May studied this situation theoretically [70, 71, 72, 73, 74]. Their results will be picked up in the discussion of the ET.

3.2 The semiconductor: TiO_2 anatase

3.2.1 General properties of TiO_2

TiO_2 crystallizes in different lattice structures. Three major structures have been reported: rutile (tetragonal, symmetry: $D_{4h}, P4_2/mnm$; the most stable and dense structure), anatase (tetragonal, symmetry: $D_{4h}, I4_1/amd$) and brookite (rhombohedrical, symmetry: $D_{2h}Pbca$) [133]. The basic structure of the scientifically and technologically important phases rutile and anatase are the same: an octahedron with a titanium center neighboring six oxygens. Therefore, in the bulk structure Ti is 6-fold and O 2-fold coordinated.

In general, the character of binding in metal oxide crystals is in-between the covalent

bonded III-V semiconductors and ionic "bonded" I-VII salts[3] [134]. Stoichiometric crystals are therefore quite insulating. The interesting semi-conducting characteristics of TiO_2 arise from imperfections of the crystals. In order to obtain a certain conductivity, different treatments have been established, which all result in n-doping of TiO_2 (see for example Refs. [135, 133]).

Rutile is easily available as single crystal and has been investigated most extensively. The feasibility of preparing defined surfaces makes the rutile structure attractive for the study of surface properties and adsorbate-rutile interfaces. A focus has been put on anatase after the observation of its high surface reactivity and due to its potential as a low-cost semiconductor in optoelectronic devices. It has mainly been studied in form of nano-crystalline particles as this is most relevant with respect to applications and as the growth of single crystals is elaborate [133]. Nevertheless, within the last ten years, the electronic structure of anatase single crystals also was investigated with surface science techniques [136, 137]. Photoelectron spectra exhibit a valence band without spectral features, which is typical for metal oxides, and which is ascribed to states with mainly O $2p$ contribution. The DOS in the band gap depends on the preparation of the surface, in particular on the Ti^{3+} concentration. The existence of Ti^{3+} results in an occupied defect state around 1 eV below the conduction band minimum (CBM) [136, 137]. Information on the bulk electronic structure of the conduction band can be obtained from DFT calculations [138, 139, 140]. These calculations reveal that the states in the lower part of the conduction band have strong Ti 3d character.

3.2.2 Nano-structured anatase

3.2.2.1 Preparation procedure

Nano-structured anatase TiO_2 films with a thickness of about 2 μm were used as the transparent semiconductor functioning as electron acceptor in the photoreaction. The development of a suitable nano-structured TiO_2 film by Grätzel et al. [5] was an essential prerequisite for the study of such interfacial electron transfer reactions with femtosecond transient absorption signals. The large inner surface area can accommodate a sufficient number of adsorbate molecules, thus providing a good signal to noise ratio in femtosecond absorption signals.

The preparation of the nano-particles and of the nano-structured films formed from these particles followed procedures described by Grätzel et al. [5, 141]. Briefly, the colloids were prepared by hydrolysis of Ti(IV)-isopropylate in aqueous solution fol-

[3]Some electronegativities for comparison: Ti: 1.54, O: 3.44; Ga: 1.81, As: 2.18; Na: 0.93, Cl: 3.16

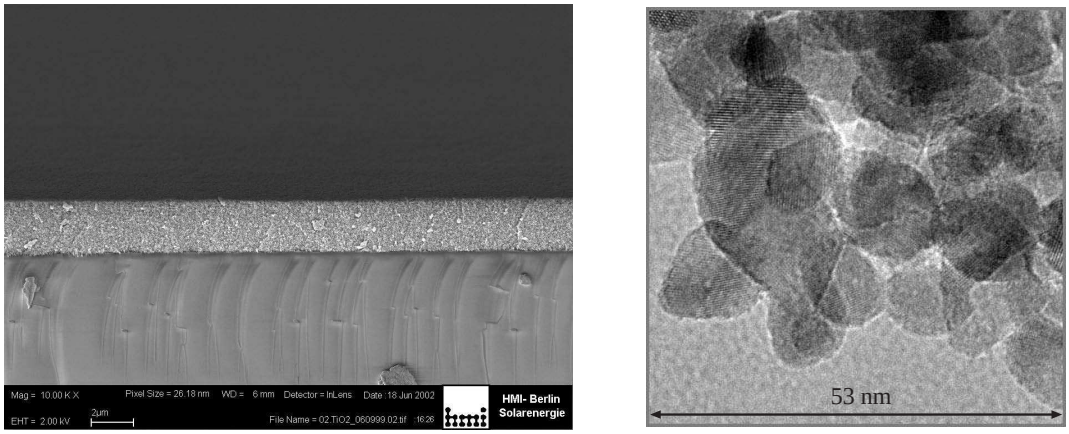

Figure 3.8: Left: SEM image of the cross-section of a porous nano-structured anatase film of about 2 μ thickness on a glass substrate. Right: TEM image of fragments of the film.

lowed by autoclaving of the acidified sol. This preparation results in nano-particles with an average diameter of about 15 nm, and with the (101) face being the dominating surface [142]. Transmission electron microscopy (TEM) as well as X-ray diffraction measurements (XRD) indicate only the anatase form of TiO_2.

For the fabrication of films on transparent substrates, the concentrated colloid solution was mixed with carbowax 20000[4], resulting in a viscous paste. Films of 30 μm thickness were drawn on glass substrates using a film applicator (Erichsen, Coatmaster 509MC). Treatment for 1 h at 450 °C under air removes the carbowax and results in high-porous nm-scale crystalline TiO_2 films. Brunauer-Emmett-Teller (BET) measurements on these films indicate a surface area of around 140 m^2/g and a mean pore diameter of 9.5 nm.

3.2.2.2 Characterization of nano-structured films

Typical scanning electron microscopy (SEM) and transmission electron microscopy (TEM) images of the anatase films are given in Fig. 3.8. The SEM image shows a cross-section of the 1.5-2 μm thick film on a glass substrate. The films are homogeneous over large areas. Fragments of the film are shown in the TEM image. The burning process creates a network of the nano-particles, whereas the size distribution of the particles and the crystal structure are being maintained according to TEM and XRD measurements.

Raman spectroscopy has also been used as morphological probe of nano-crystalline TiO_2 as both phases show characteristic Raman peaks [143, 144, 145]. Fig. 3.9 shows the Raman spectrum of powder from a burned TiO_2 film, which was scratched off

[4]Carbowax is the polyethylene glycol H-(CH_2-CH_2-O)$_n$-OH, with an molar mass of 20000.

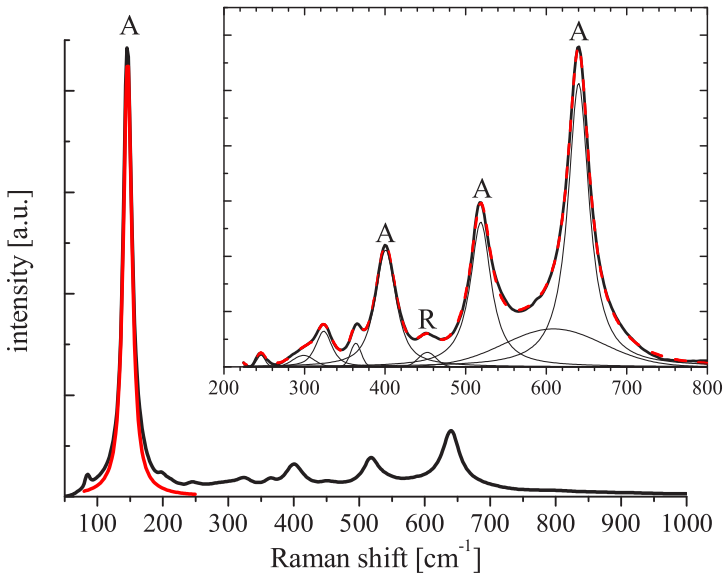

Figure 3.9: Raman spectra of the TiO_2 film (thick solid line). Characteristic anatase peaks are marked with "A". The spectrum in the inset is fitted with ten peaks (total fit: red dashed line, single peaks: thin solid line).

the glass substrate. The spectrum exhibits the characteristic anatase peaks [143, 144, 145] marked with "A": the intense peak at 146 cm^{-1} and three strong bands at 400, 520 and 639 cm^{-1} . The minor peak at 452 cm^{-1} , which is marked with "R", can be assigned to the rutile phase. Thus, there is a minor fraction of rutile present in the film after the burning process. The integral over this rutile peak is 2.8% of the 639 cm^{-1} and 0.6% of the 146 cm^{-1} peak area. Peak positions and the line widths of Raman peaks depend on the particle size [146, 147, 144]. Estimating the particle size according to the empirical relations of Refs. [147, 144] results in diameters of 7-8 nm, which is around half of the size estimated from TEM measurements. This difference between the estimation from Raman spectroscopy and an imaging technique has also been observed by comparison of Raman spectra with atomic force microscopy [148].

For the functioning of the DSSC, the charge migration within the TiO_2 network is essential, wherefore this subject has been studied extensively (see for example Refs. [149, 150, 151]). However, the inter-particle electron migration is not relevant for the investigation of the electron injection.

Small semiconductor colloids show size quantization effects like an increased band gap. The electronic structure of particles with a diameter of 10 nm and more is close to the bulk structure of single crystals [6]. The optical gap of the semiconductor

is a measure for quantization effects. However, the shape of the optical absorption edge depends on several features of the electronic structure, like the dispersion of the valence and the conduction band (reflected by the joint density of states), the nature of the band gap (direct or indirect), the energy-dependence of the transition matrix elements, and the presence of excitonic effects [152, 153]. Assuming parabolic bands, the standard relation between the absorption coefficient $\alpha(\omega)$ and the photon energy $\hbar\omega$ reads [152]

$$\sqrt{\alpha(E)E} = \alpha_0(E - E_{gap}), \tag{3.1}$$

with E_{gap} denoting the band gap. An absorption edge of the Urbach type, however, shows an exponential behavior [153]:

$$\alpha(E) = \alpha_0 \, exp(-\sigma\frac{E_{gap} - E}{kT}). \tag{3.2}$$

Fits of the absorption spectra according to Eqs. 3.1 and 3.2 reveal band gaps of 3.35 and 3.55 eV, respectively. The latter value is 0.1 eV above the value observed for anatase single crystals [153]. Thus, the quantization effects are negligible in the investigated system.

3.2.2.3 Choice of the glass substrate

Transient absorption measurements detect changes in the intensity of an probe pulse induced by a pump pulse. Coherent contributions to the signal at temporal overlap of the pulses are an inherent problem of this technique [154, 155]. These non-resonant effects superimpose the "regular" pump-probe signal, the so-called sequential contributions. Details of this effects will be discussed in section 4.1.1.4.

In the case of transient absorption measurements under vacuum conditions, the glass substrate is most likely to generate coherent signals. In order to reduce these contributions, different thin glass substrates were used: 50 μm thick AF45 glass and 40 and 70 μm thick D263 glass (Schott Displayglas). By use of these glasses, the weak pump pulses used in this study give rise to less than 0.1 mOD probe absorbance change, which is at least a factor of ten less than the sequential signal.

It has been observed that the alkali content of the glass substrate affects the dye-TiO_2 interface due to diffusion of alkali atoms into the anatase film during the burning process. This effect will be discussed in section 4.4.2. In order to avoid this effect, alkali-free AF45 (alkali content $< 0.2\%$[5], AF stands for "alkali-free") has been used as standard, whereas measurements on the D263 glasses with low alkali content (Na_2O: 6.4%, K_2O: 6.9%) did not show systematic deviations compared to AF45 glass.

[5]Information obtained from Schott Displayglas.

Photoelectron spectroscopy requires conducting samples, therefore 500 nm SnO_2:F on 1 mm float glass has been used as substrate for these measurements.

3.2.3 Sensitization and transfer into UHV

The investigated perylene dyes are adsorbed onto the colloidal semiconductor by simply immersing the latter for 5-20 min at room temperature into a dye solution, typically 10^{-4} M in toluene, resulting in an absorbance of 0.5-0.8 OD at 440 nm. The kinetics of the adsorption shows a dependence on the anchor group. The dyes with a carboxylic group (besides DTB-Pe-tripod) sensitized the semiconductor about three to five times faster compared to the phosphonic acids.
The adsorption reaction inside the porous film is diffusion-limited. Shaking of the dye solution while the sample is immersed results in faster sensitization.
Samples for UPS measurements were colored to an absorbance of 1.0-1.2 OD. Both treatments did not saturate the binding sites in the anatase film. Prior to adsorbing the dye the TiO_2 film was brought to 450 °C for 45 min in laboratory ambient. The dye-covered TiO_2 electrode was rinsed with dried solvent, blown off with Argon, and then quickly transferred via a load-lock chamber into an UHV chamber with a base pressure in the 10^{-10}-10^{-9} mbar range. The design of the chamber is described in detail in section 2.1.

The pump-probe measurements were carried out under UHV conditions since the samples were found to be stable over hours during the measurements, besides some initial drop in signal strength. This reassuring stability in vacuum was rather different from the gradual degradation of otherwise identical systems if exposed to the laboratory ambient. For example it is known that water reacts with the cationic state of perylene, thereby splitting the aromatic ring system [156]. Also the stability during storage under UHV conditions of the samples is clearly improved as no degradation could be observed over some month. Comparable good stability even over years was found for a sample transferred into an evacuated ampule which was filled with an Argon atmosphere and sealed with a burner. Additionally, vacuum conditions provide a simpler system by excluding environmental effects.

3.3 Characterization of the adsorbate-surface binding configuration: FT-IR spectroscopy

Different experimental techniques have been applied to investigate the nature of the binding mode of carboxylic acids to titanium oxide surfaces. IR spectroscopy has been performed to study the adsorption of e.g. ruthenium (II) bipyridyl dicar-

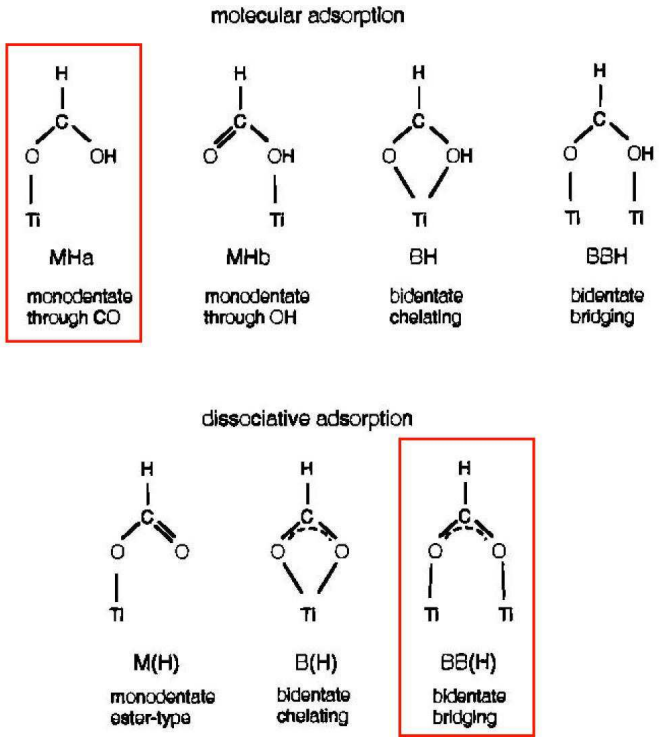

Figure 3.10: Possible binding configurations of formic acid (HCOOH) on anatase (110) [taken from Ref. [166]]. The most likely binding modes are marked with red boxes.

boxylic acid [157], (2,2'-Bipyridyl-4,4-dicarboxylic acid)ruthenium(II) [158], benzoic acid [158], 4,4'-Bis(2-sulfostyryl)biphenyl [159], and the so-called black dye [160]. These molecules show in unison an absorption band around 1700cm^{-1} arising from the C=O stretch mode of the un-dissociated carboxylic group. This band disappears when the molecules are linked to nano-structured anatase, rutile or amorphous TiO_2, which has been interpreted as bi-dentate bridging coordination [157, 158, 159]. Also formic acid [161, 162, 163], which is the anchor group of some of the chromophores investigated here, benzoic acid [164] and bi-isonicotinic acid [165] have been found to adsorb on rutile (110) under dissociation of a proton in a bi-dentate bridging coordination.

Kim et al. [167] investigated the adsorption from gas phase of formic, acetic and propionic acid on nano-crystalline anatase by means of temperature-programmed desorption (TPD) measurements and IR spectroscopy. Besides weakly adsorbed molecules, which desorbe at room temperature under vacuum conditions, the TPD spectra indicate two adsorbed species for carboxylic acids. The stronger binding configuration could be identified to be of dissociative nature.
Vittadini et al. [166] studied the adsorption of formic acid on the anatase (101) surface theoretically under consideration of different configurations for both molecular and dissociative adsorption (see Fig. 3.10). The (101) crystal face is also the most frequent surface in the nano-structured film used in this work. These authors found the bi-dentate bridging configuration to be the most stable *dissociative* ad-

sorption mode for a clean surface. The energetically favored *un-dissociative* binding configuration is mono-dentate binding through the carbonyl group accompanied by a hydrogen bond between the proton of the anchor group and a surface oxygen atom [166]. These two configurations are marked with red boxes in Fig. 3.10. As pointed out in Ref. [166], the un-dissociative binding mode is stabilized by the hydrogen bond, which requires a two-fold coordinated, i.e. an unprotonated, oxygen atom at the surface. However, the concentration of two-fold coordinated oxygen atom is unknown. In view of the wet chemistry preparation method, it is likely that there is no significant amount of unsaturated surface oxygen present.
In addition to the clean surface, Vittadini et al. [166] modeled the adsorption of formic acid on hydrated surfaces[6]. The most stable configuration was found to be dissociative and mono-dentate, whereas the configuration is stabilized by hydrogen bonds. In other words, one of the carboxylate oxygen atoms binds to a five-fold Ti atom, and the second one via a hydrogen bond to a surface hydroxyl group [166]. As the adsorbate/surface geometry is fixed via two bonds this configuration can be seen as a pseudo-bridging form [170].
Although a model describing a hydrated surface is more realistic than a clean one, it still might be too idealistic for comparing it with a nano-structured metal oxide, which has been prepared and sensitized by wet-chemistry techniques. Ref. [166] also gives an idea of the influence of alien atoms on the energetics of the adsorbate-surface binding: the presence of Na^+ in the vicinity of $HCOO^-$ stabilizes the bi-dentate bridging by as much as 0.65 eV.

Fig. 3.11 shows the IR absorbance spectrum in the range of 1000 to 2000 cm^{-1} of 2,5,8,11-tetra-tertiary-butyl-perylene (TTB-Pe) powder [19], DTB-Pe-COOH (0.7 mg in 300 mg KBr) and the difference spectrum of DTB-Pe-COOH sensitized and un-sensitized anatase. The samples for the latter spectrum have been prepared analogue to the samples for the time-resolved measurements. The un-sensitized reference sample has been brought to pure solvent while dye-coating the other sample. Prior to measurement, both samples have been brought sufficiently long under UHV conditions to evaporate the solvent within the sponge-like film. After flooding the samples with nitrogen, the TiO_2 films were scratched off the glass substrate and brought into the nitrogen flooded FT-IR spectrometer. Pure perylene shows absorption bands up to 1600 cm^{-1} [171, 172], which arise mainly from in-plane vibrational modes [124]. In the spectral window shown above, the IR absorption of TTB-Pe and pure perylene [171] agree well besides the characteristic bands arising from the tertiary-butyl groups ($\delta_{as}(CH_3)$ at 1477 cm^{-1} and $\delta_s(C(CH_3)_3)$ at 1362 cm^{-1}).
The most obvious difference between the spectra of DTB-Pe-COOH and TTB-Pe is a strong band around 1680 cm^{-1}, which is characteristic for the C=O stretch

[6]Water is assumed to adsorb molecular rather than dissociative on the most frequent anatase surfaces (101) and (100)/(010) [168, 169].

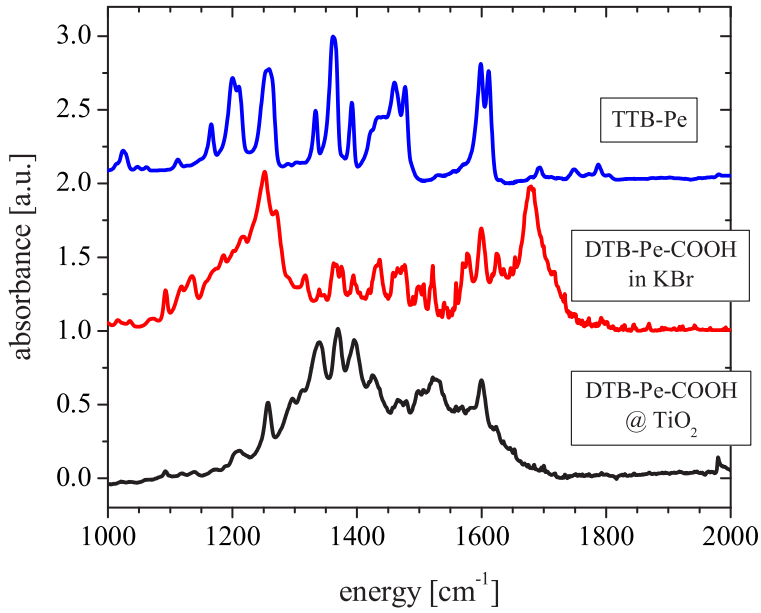

Figure 3.11: FT-IR absorption spectrum of TTB-Pe powder [19], DTB-Pe-COOH in KBr, and the difference spectrum of DTB-Pe-COOH-sensitized and un-sensitized nano-crystalline anatase.

mode of the carboxylic group [157, 158, 159, 160]. The absence of this signature in the difference spectrum of sensitized and un-sensitized anatase indicates a binding configuration without a C=O double bond. This excludes mono-dentate binding for dissociative adsorption as well as mono-dentate binding through the OH group for the case of molecular adsorption (see Fig. 3.10).

The coordination of the COO^- group to metal cations has been studied by the energy splitting of antisymmetric $\nu_{as}(COO^-)$ and symmetric $\nu_s(COO^-)$ stretching vibrations [173, 170]. Bauer *et al.* observed two peaks at 1615 cm^{-1} and 1350 cm^{-1} for the black dye adsorbed on anatase, which were assigned to the $\nu_{as}(COO^-)$ and $\nu_s(COO^-)$, respectively. The IR spectrum of adsorbed DTB-Pe-COOH shows broad absorption rather than distinct peaks at that spectral positions. Despite its unstructured shape, this broad absorption between 1300 and 1600 cm^{-1} is a reproducible feature of the spectrum. In principle, it should be possible to distinguish molecular and dissociative adsorption by the energy difference between $\nu_{as}(COO^-)$ and $\nu_s(COO^-)$, as this splitting depends on the local symmetry of the COO^- group [173, 170]. The presence of a broad absorption between 1300 and 1600 cm^{-1} therefore might reflect an inhomogeneous distribution of configurations with different splitting of $\nu_{as}(COO^-)$ and $\nu_{as}(COO^-)$.

In conclusion, the IR spectra show a disappearance of the C=O stretching mode due

to adsorption. Bi-dentate chelating binding configurations, which do not exhibit a C=O bond, can be ruled out due to the unfavorable energetics of this configuration (negative adsorption energy) [166]. Thus, the dissociative bi-dentate bridging geometry and the un-dissociative "mono-dentate trough carbonyl" geometries (red boxes in Fig. 3.10) remain the most likely configurations. It should be noted that both geometries have bi-dentate character. In the latter case, this arises from the stabilization by the hydrogen bonding.

The adsorption configuration of the phosphonic acid can hardly be clarified by IR spectroscopy, as the characteristic P-O vibrations overlap with the TiO_2 absorption. The binding modes of the phosphonic acids is discussed in section 4.2.

3.4 Energy level alignment at the surface

3.4.1 Introduction

The relative position of molecular and semiconductor electronic states is a key parameter of the interface and the ET dynamics. According to the Fermi Golden rules expression given in Eq. 1.2, the ET rate is proportional to the available density of acceptor states. In addition to the DOS factor, the position of the donor might enter Eq. 1.2 via the coupling term as well. This could be the case if the character of the bulk states and thus the electronic coupling to the adsorbate changes with energy.

The level alignment at the surface has been addressed with ultraviolet photoelectron spectroscopy (UPS) and X-ray photoelectron spectroscopy (XPS). The combination of both techniques allows the differentiation of band bending and surface dipole-layer effects contributing to the interfacial electronic structure, as discussed by K. Seki *et al.* [174]. Hitherto, there are only few publications on the interfacial electronic structure of molecules adsorbed on nano-structured TiO_2 [175, 176].
The charging of the samples during the experiment is a well-known problem in the investigation of systems with poor conductivity by photoelectron spectroscopy. Such a charging, which manifests in a shift of the spectra to higher binding energy, is observed for the nano-structured films at room temperature. However, the conductivity of nano-structured anatase films increases strongly with temperature [177]. It has been found that there is a temperature window (80-170 °C), which provides sufficient conductivity of the semiconductor and which is still below the desorption and decomposition threshold of the adsorbate. The latter aspect has been carefully investigated. The details are given in the appendix A.2.

It should be noted that the (inelastic) escape depth of photoemitted electrons is around 1 nm for UPS and about 2 nm for XPS [178], i.e. in any case far less than

the diameter of a single colloid. Thus, UPS and XPS address the outer surface of the colloidal film, whereas optical measurements applied in this study integrate over the whole - and thus mainly inner - surface of the sample. It is assumed that the electronic structure of the outer surface is not significantly different to the average of the porous film.

3.4.2 Valence electronic structure: UPS

Fig. 3.12 shows UPS spectra of un-sensitized and DTB-Pe-COOH sensitized colloidal anatase films. The excitation energy is 21.22 eV (He-I). The energy axis of the spectra is referenced to the Fermi energy (E_F). The left panel shows the energy distribution curves (EDCs) of the whole energy range. The EDC of the pure colloidal film exhibits the O $2p$ valence band in the range 3 to 9 eV below E_F, similar to the valence band of anatase single crystals [136, 137]. The valence band is followed toward higher binding energies by an intense onset of secondary electrons. The EDCs of both samples were taken subsequently with the same adjustment and alignment, which is critical with respect to the signal strength.
The right panel of Fig. 3.12 shows the details around the energy range of the band gap. The difference of the EDCs (red solid line) exhibits two peaks around the valence band maximum (VBM) separated by 1.6 eV. These peaks can be assigned to the HOMO and the next lower states of the adsorbed perylene derivative. The separation of the peaks as well as the relative amplitudes agree well with UPS measurements of perylene in the gas phase [179] and of perylene crystals [180].

The molecular peaks in the difference of the EDCs are also in good agreement with the calculated density of states (DOS), which is shown for different perylene derivatives in Fig. 3.13. The calculated spectrum was obtained by the convolution of the energy eigenvalues with a normalized Gaussian of 500 meV FWHM. Therefore, a single state gives rise to a peak with amplitude one. The DOS of the occupied states below -6 eV exhibits a very similar structure compared to the experimental results. Fig. 3.13 reveals that the highest peak origins from the HOMO only, whereas the second peak at about 1.6 eV higher binding energy results from three almost degenerate states (HOMO-1 to HOMO-3), giving rise to the experimentally observed peak ratio of about 1:3.

The position of the valence band maximum (VBM) is determined to be at 3.3 eV by a linear fit of the low-binding energy threshold of the EDC from the pure anatase sample. The linear absorption spectrum of anatase reveals an optical gap of 3.35 eV. Thus, E_F almost coincides with the conduction band minimum (CBM). Now we can estimate the position of the molecular excited state by adding the optical excitation energy to the position of the HOMO. The black dash-dotted line in Fig. 3.12 is

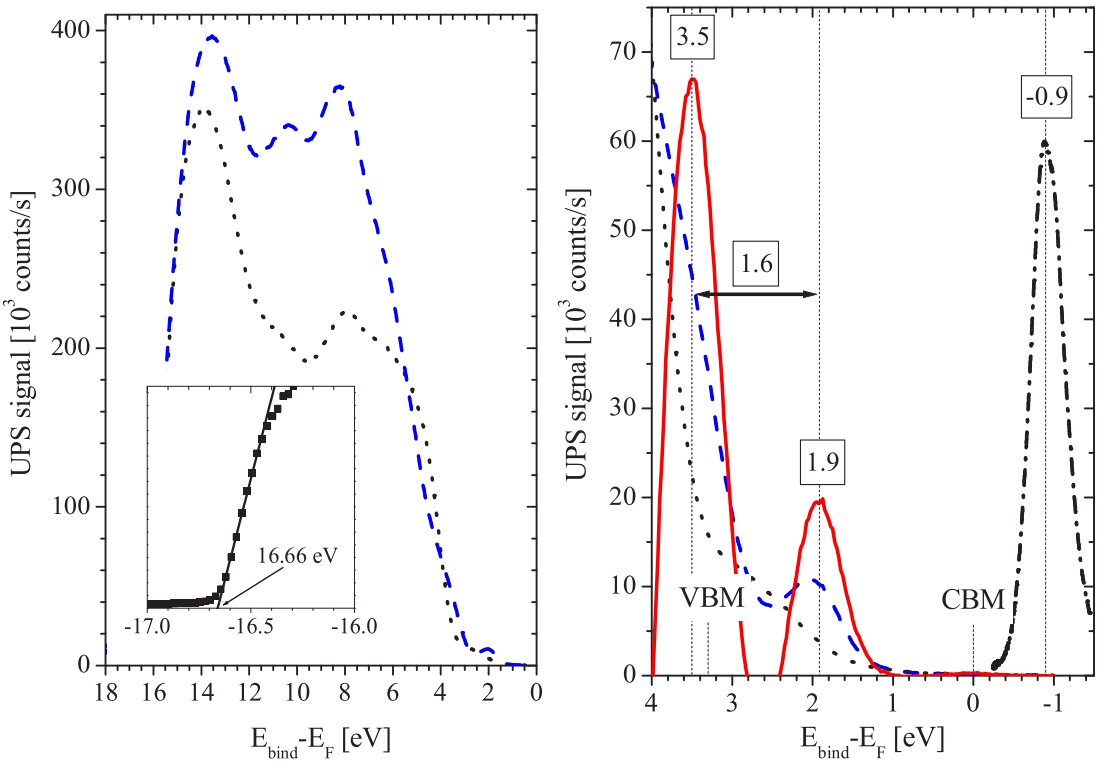

Figure 3.12: Left panel: UPS spectrum (He-I) of a DTB-Pe-carbonic acid-sensitized (blue dashed line) and an un-sensitized nano-structured anatase film (black dotted line). The inset shows the secondary edge of the sensitized film taken with a bias of 4 V. Right panel: Detailed view of the range around the band gap. The difference spectrum (red solid line, enlarged by a factor of 3) shows the HOMO and the HOMO-1, separated by 1.6 eV. The position of the molecular excited state (black dash-dotted line), i.e. the donor state in the electron injection process, is estimated by adding the absorption spectrum to the center of the HOMO at -1.9 eV.

the absorption spectrum of the adsorbed dye relative to the HOMO maximum at 1.9 eV binding energy. This spectrum peaks 900 meV above E_F (= E_{CBM}). The vibrational ground state is about 100 meV lower. Thus, the spectrum at positive energies in Fig. 3.12 gives a good idea of the relative position of the donor orbital of the excited singlet state of perylene with respect to the conduction band levels of TiO_2. The reorganization energy is expected to be 300 meV or smaller for electron injection from the excited state of the perylene chromophore. Therefore, all the Franck-Condon factors of the ET reaction should indeed be realized in parallel for the ET reaction. The electronic coupling alone should control the electron injection time in this system, as outlined in section 1.2.2 and in Refs. [7, 71, 70].

The energy axis with respect to E_F is related to the vacuum level via the work function of the sample. The inset in the left panel shows the secondary edge of the sensitized sample. The work function can be obtained by a linear fit of the EDC

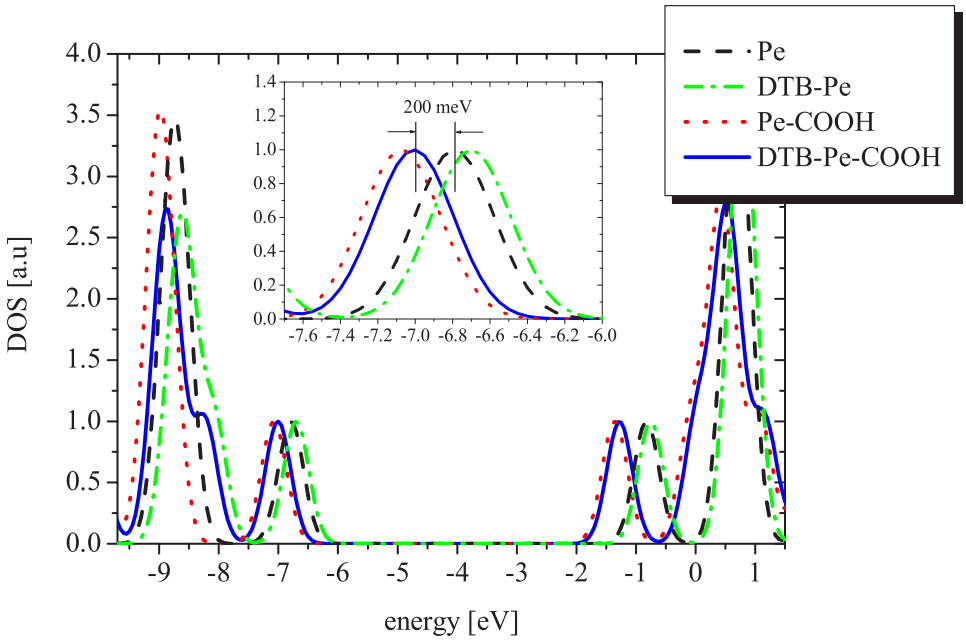

Figure 3.13: Calculated DOS of Pe, DTB-Pe, Pe-COOH, and DTB-Pe-COOH. The different plots show the effects of the DTB groups and the carboxylic group on the position of the HOMO relative to vacuum.

cutoff. The fit intersects the energy axis at 16.66 eV. In order to obtain the work function of the sample, this value has to be corrected by half of the energy resolution (100 meV) of the setup. Thus, the work function, i.e. the position of E_F below the vacuum level, is 21.22 eV - (16.66 eV - 0.05 eV) = 4.6 eV.

The corresponding ionization energy of DTB-Pe-COOH on the surface is therefore 6.5 eV. This is about 500 meV less compared to the perylene chromophore in the gas phase [179]. The calculated DOS shown in Fig. 3.13 reveals that the ionization energy of DTB-Pe-COOH (blue solid line) should be 200 meV higher compared to pure perylene (black dashed line). Thus, the lower ionization of the adsorbed perylene derivative arises probably from the presence of the surface rather than the substituted groups.

As mentioned above, the UPS measurement reveals that the Fermi energy coincides with the CBM, which is consistent with other photoelectron measurements on both anatase single crystals [136, 137] as well as nano-structured films [175]. However, it is not possible that such a high level of E_F is the equilibrium level of the nano-structured semiconductor in the dark, as the DSSC otherwise could not show any photo-voltage [151]. Thus, the observed E_F is only a quasi-Fermi level, which arises from the filling of trap states in-between the dark equilibrium potential and the CBM due to the UV excitation. These trap states are known to have lifetimes of up to seconds [8].

3.4.3 Core states: XPS

The discussion of the level alignment in the previous section bases on the assumption that the adsorption of the molecule does not shift the energetic position of the semiconductor states. Such a shift might arise from a surface dipole induced by the adsorption or from the change of an already existing dipole due to adsorption. As pointed out by Seki *et al.* [174] and Schlaf *et al.* [181], such a shift cannot be ascertained by any change of the work function as the vacuum level itself is a surface property. A surface dipole can only be detected by a change in the energetic position of core levels of the substrate.

Fig. 3.14 shows XPS spectra of the Ti 2p, O 1s and C 1s core levels for the same samples as considered in Fig. 3.12. Fits of the data are given as solid lines and the fit parameters are summarized in table 3.1. The available energy resolution allows the detection of peak shifts of about 100 meV. According to the fit parameters, the core levels of the substrate, Ti 2p and O 1s, agree within 20 meV. This demonstrates that the adsorption of the dye induces no significant change in the electronic potential at the interface. This finding justifies belatedly the estimation of the injection level from the UPS data.

	Ti 2p pure TiO_2 / dye+TiO_2	O 1s pure / dye	C 1s pure / dye
binding energy [eV]	459.37 / 459.39	530.71 / 530.72	285.07 / 285.01
$2p_{1/2}$ - $2p_{3/2}$ [eV]	5.75 / 5.76	- / -	- / -
FWHM [eV]	1.446 / 1.435	1.66 / 1.65	1.95 / 1.73
Amp.	3818 / 2460	4516 / 2814	161 / 545
asym.	-0.052 / -0.052	-0.087 / -0.128	- / -

Table 3.1: Fit parameters of the XPS spectra of shown in Fig. 3.14. "Asym." denotes an asymmetry parameter. The dye used in this experiment is DTB-Pe-COOH.

The UPS and XPS measurements were conducted for all perylene dyes. The fit parameters of all XPS data are summarized in table A.1 in the appendix. The comparison of the data of the different dyes reveals that the alignment of the molecular states with respect to the semiconductor states is independent of the bridge-anchor group (within the experimental uncertainty of +/- 100 meV).
This behavior of the perylene derivatives is slightly different compared to the adsorption of Ru-complexes where a weak surface dipole of 200 meV has been observed [175].

Besides the absence of a detectable peak shift, the XPS data shown in Fig. 3.14 contains further information on the system:

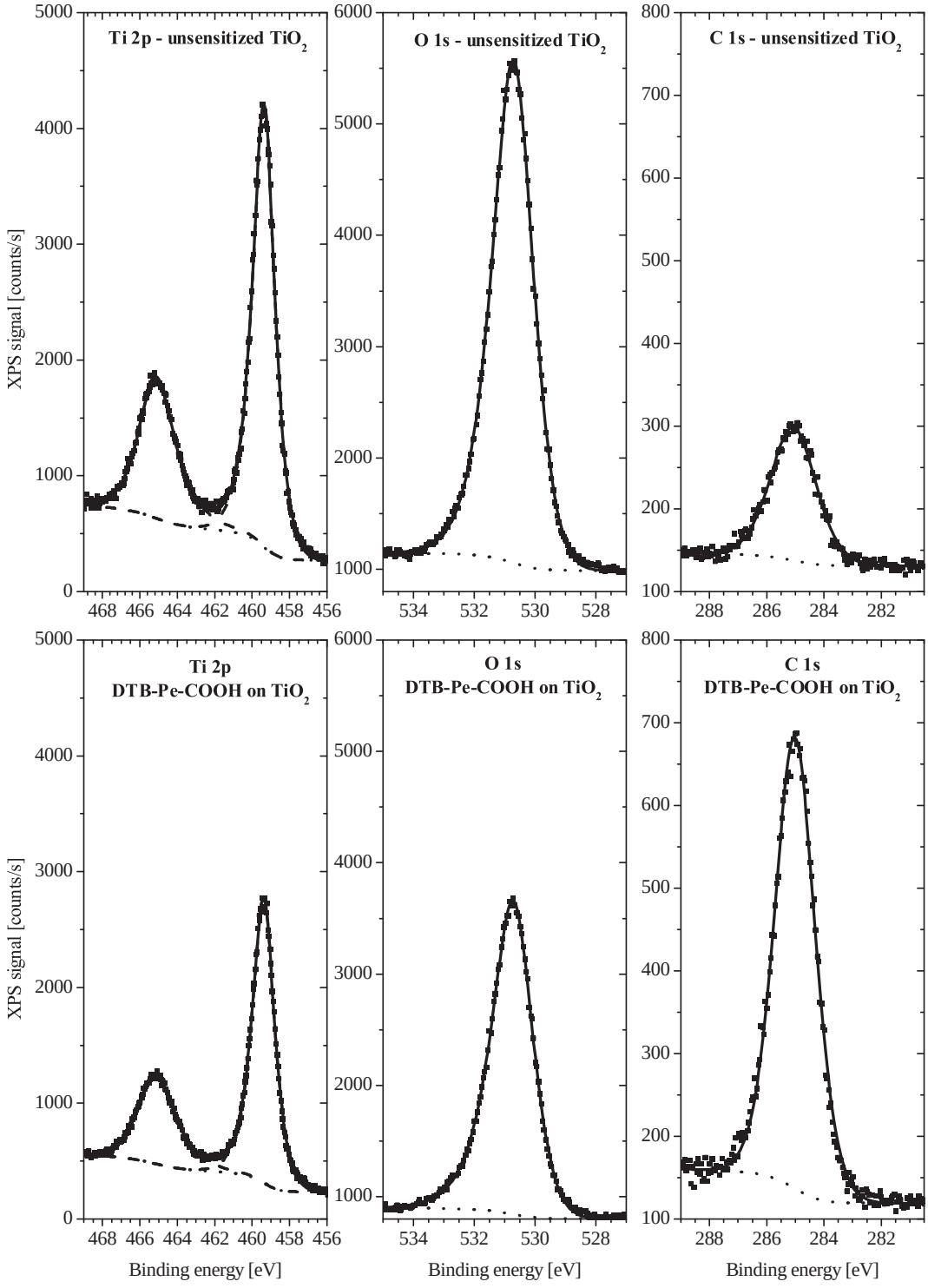

Figure 3.14: Ti 2p, O 1s and C 1s (from left to right) XPS core level spectra of the un-sensitized (top) and the dye loaded (bottom) anatase film. Data points are given as squares, fits as solid lines. The fit parameters are summarized in Table 3.1.

- There is no signature of a Ti^{3+} state, which is typical for reduced surfaces. This state would appear with a chemical shift of 2.1 eV to lower binding energy [136, 175].

- The shape of the O 1s peak changes due to the adsorption of the dye. The Ti 2p and the O 1s peaks have been fitted with asymmetric peak functions (although there is no reason for the assumption of asymmetric line shapes). In the case of the oxygen, the asymmetry indicates contributions from a second oxygen species with slightly higher binding energy. As the contribution is small, a fit with two symmetric peak functions does not converge in a reproducible manner. Therefore, the asymmetry is allowed. It is interesting to note that the asymmetry of the oxygen peak verifiable changes due to the adsorption of the dye. This might indicate contributions from the carboxylate oxygens, as these can be expected at higher binding energy [182].

- There is a significant C 1s peak from the un-sensitized anatase film. This carbon arises most likely from incompletely oxidized Carbowax used in the preparation of the anatase films. There is no information to which extent this carbon affects the surface electronic structure or the adsorption of the dyes. The energetic position of the C 1s peak is close to 285 eV and therefore suggests the presence of either elementary carbon or of carbon with sp^2-hybridization. If the carbon is homogeneously distributed or accumulated on the surface is an additional open question.

  Whatever the role of this carbon is with respect to the interfacial ET, it is inherent for the nano-structured films used for DSSC. In the following chapter, the ET dynamics is studied by means of systematic variation of molecular properties. The most important demand on the semiconductor samples is their reproducibility. This aspect has been elaborately studied and is discussed in section 4.4.2. However, such parameters as the amount of carbon on the surface most likely differ between the samples investigated in different research groups. This might be one of the reasons why such a large spread of electron injection times have been reported for different systems (see section 1.3).